Three-Bed PVSA Process for High-Purity O_2 Generation from Ambient Air

Jeong-Geun Jee, Sang-Jin Lee, Min-Bae Kim, and Chang-Ha Lee
Dept. of Chemical Engineering, Yonsei University, Shinchon-dong, Seodaemun-gu, Seoul, 120-749, Korea

DOI 10.1002/aic.10548
Published online August 4, 2005 in Wiley InterScience (www.interscience.wiley.com).

A three-bed PVSA (pressure vacuum swing adsorption) process, combining equilibrium separation with kinetic separation, was developed to overcome the 94% O_2 purity restriction inherent to air separation in the adsorption process. To produce 97+% and/or 99+% purity O_2 directly from air, the PVSA process with two zeolite 10X beds and one CMS bed was executed at 33.44–45.60 to 253.31 kPa. In addition, the effluent gas from the CMS bed to be used for O_2 purification was backfilled to the zeolite 10X bed to improve its purity, recovery, and productivity in bulk separation of the air. PVSA I, which made use of a single blowdown/backfill step, produced an O_2 product with a purity of 95.4–97.4% and a recovery of 43.4–84.8%, whereas PVSA II, which used two consecutive blowdown/backfill steps, produced O_2 with a purity of 98.2–99.2% and a recovery of 47.2–63.6%. Because the primary impurity in the O_2 product was Ar, the amounts of N_2 contained in the product were in the range of 4000–5000 ppm at PVSA I and several tens of ppm at PVSA II. A nonisothermal dynamic model incorporating mass, energy, and momentum balances was applied to predict the process dynamics. Using the linear driving force (LDF) model with constant diffusivity for the equilibrium separation bed and a modified LDF model with concentration dependency of the diffusion rate for the kinetic separation bed, the dynamic model was able to accurately predict the results of the experiment. © 2005 American Institute of Chemical Engineers *AIChE J,* 51: 2988–2999, 2005
Keywords: high-purity O_2, PVSA, backfill step, blowdown step, CMS, zeolite 10X

Introduction

In the study of air separation, classical cryogenic distillation has been widely recognized as one of the most common methods of O_2 production. However, this technology is not compatible with relatively small size [<100 TPDc (tons per day contained)] O_2 plants.[1] Recently, the development of highly selective adsorbents such as LiX, LiAgX, and LiCaX has contributed to the possibility of manufacturing up to 200 TPDc by vacuum swing adsorption (VSA) process, at a power consumption rate competitive with that of cryogenic distillation.[2]

During the last 30 years, commercial applications for adsorptive O_2 generation from ambient air using several molecular sieve zeolites have been expanded.[3-7] However, because air contains a small amount of Ar, which has physical properties similar to those of O_2, the product generated from the zeolite bed typically contains a substantial amount of the Ar impurity. Therefore, in the equilibrium separation process using zeolites, O_2 purity is limited to about 94% purity. For this reason, O_2 produced by adsorption technology typically has 90–93% purity, of which 4–5% is Ar and 2–6% N_2, and is generally used in many chemical processes such as the biological treatment of wastewater, steel industries, paper and pulp industries, and glass-melting furnaces.[8,9]

In addition to these industries, there is a great demand for O_2 with a purity level of 99% or higher in other applications, such as welding and cutting processes, plasma chemistry, ozone generation, medicine, combustion, cylinder filling, and O_2 for

Correspondence concerning this article should be addressed to C.-H. Lee at leech@yonsei.ac.kr.

Table 1. Cyclic Sequences of Three-Bed PVSA Process for Air Separation and O_2 Purification*

PVSA I

Step	[1]	[2]	[3]	[4]	[5]	[6]	[7]	[8]
1st zeolite bed	[PR ↑]	[AD ↑]		[DPE ↑]	[VU ↓]		[BF ↓]	[PPE ↓]
2nd zeolite bed	[VU ↓]		[BF ↓]	[PPE ↓]	[PR ↑]	[AD ↑]		[DPE ↑]
CMS bed	[BD ↓] product	[PR ↑] (O_2 supply from 1st zeolite bed)	[AD ↑]	[ID]	[BD ↓] product	[PR ↑] (O_2 supply from 2nd zeolite bed)	[AD ↑]	[ID]

PVSA II

Step	[1]	[2]	[3]	[4]	[5]	[6]	[7]	[8]	[9]	[10]
1st zeolite bed	[PR ↑]	[AD ↑]		[DPE ↑]	[VU ↓]		[BF1 ↓]	[PPE ↓]	[BF2 ↑]	
2nd zeolite bed	[VU ↓]	[BF1 ↓]		[PPE ↓]	[BF2 ↑]	[PR ↑]	[AD ↑]	[DPE ↑]	[VU ↓]	
CMS bed	[BD2 ↓] product	[PR ↑] (O_2 supply from 1st zeolite bed)	[AD ↑]	[ID]	[BD1 ↓]	[BD2 ↓] product	[PR ↑] (O_2 supply from 2nd zeolite bed)	[AD ↑]	[ID]	[BD1 ↓]

* ↑, Cocurrent flow; ↓, countercurrent flow; PR, pressurization step; AD, adsorption step; DPE, depressurizing pressure equalization step; VU, vacuum step; BF1, first backfill step; BF2, second backfill step; PPE, pressurizing pressure equalization step; ID, idle step; BD1, first blowdown step; BD2, second blowdown step.

breathing at high altitudes in pressurized space suits or in various laboratory applications.[10]

Recently, because of the reduction and sequestration of CO_2, O_2 inhalation combustion processes have been developed extensively for use in, among others, the iron, steel, and incineration industries.[11] In these industries, O_2 needs to be at least 95% pure to be used cost-effectively in fuel combustion because of the carbon tax placed on CO_2 capturing. Moreover, the recommended amount of N_2 impurity contained in an O_2 product for controlling the amount of NO_x released under the allowable exhaust standard is $<1\%$.

As a result of extensive industrial demand for high-purity O_2, several adsorption processes have been developed, the patents for which involve a two-stage process consisting of zeolite beds for nitrogen removal and carbon molecular sieve (CMS) beds for the removal of argon and nitrogen impurities.[12-15] Knaebel and Kandynin[14] posited that an O_2 product with 99.6% purity and 25% recovery could be obtained from a five-step, four-bed PSA using two consecutive blowdown steps. They also noted that a desirable level of productivity would be about 11 $Nm^3\ m^{-3}\ h^{-1}$. Hayashi et al.[16] observed that an O_2 recovery ratio of up to 50% was obtained during the production of O_2 with a purity of 99% through a connection between the zeolite Ca-X bed and the CMS bed, each of which consisted of three beds. Recently, Jee et al.[17] reported that a two-bed PSA process with CMS could purify 95% O_2 to 99.8% purity with 78% recovery. However, these processes mentioned need to overcome the additional equipment costs to set up the purification unit and the significant product loss for applications as a O_2 balance unit with a cryogenic unit and a direct on-site unit.

In this study, a three-bed pressure vacuum swing adsorption (PVSA) process, consisting of two zeolite 10X beds and one CMS bed, was developed to produce high-purity O_2 with $<1\%$ N_2 impurity from ambient air. The first two zeolite 10X beds functioned to achieve bulk separation of the air. Thereafter, the CMS bed purified the O_2 supplied from the zeolite 10X beds. To increase the purity and productivity of the PVSA process, we proposed refluxing the waste from the CMS bed into the zeolite 10X beds by using vacuum pressure in the zeolite bed. As a result, the PVSA process could be operated with one blower/compressor and one vacuum pump.

A nonisothermal dynamic model incorporating mass, energy, and momentum balances was used to predict dynamic behavior in the PVSA process, combining equilibrium separation with kinetic separation. The linear driving force (LDF) model with constant diffusivity for the equilibrium separation bed and the concentration-dependent rate model for the kinetic separation bed were used concurrently to the dynamic model.

Description of the PVSA Process

Two different three-bed PVSA cycles were proposed to produce 97+ and 99+% O_2 generation from ambient air. The cyclic sequences of the proposed PVSA processes are represented in Table 1.[18]

In the case of the PVSA I process, the two zeolite beds were operated as a PVSA sequence containing pressure equalization and single backfill steps from the CMS bed. Meanwhile, the CMS bed was operated as a PSA sequence with one blowdown step. As noted in Table 1, when the first zeolite bed produced highly concentrated oxygen containing impurities such as Ar and N_2, the CMS bed was pressurized by the product from the zeolite 10X bed until it reached the adsorption pressure of the bed and this pressure was maintained throughout the adsorption step of the process. During the adsorption step, Ar and N_2 impurities were removed by the kinetic selectivity of CMS, although the concentration of O_2 effluent from the CMS bed was much higher than that of the ambient air. The effluents from the adsorption step of the CMS bed were supplied to the second zeolite bed and regenerated by vacuum pressure, as a backfill step to partially pressurize the zeolite bed with the concentrated oxygen. This step prevented any of the gas supplied by the zeolite bed from being wasted in the CMS bed. During the pressure equalization step in the zeolite bed, the CMS bed underwent the idle step for the cyclic symmetry of the process. The idle step provided the contact time for the diffusion of O_2.[17] Then, during the pressurization step of the second zeolite bed, the CMS bed produced purified oxygen at the blowdown step.

In the case of the PVSA II process, a two-stage blowdown step of the CMS bed, followed by a fractionation of its oxygen product, was implemented to increase O_2 purity to 99%. Be-

cause Ar and N_2 impurities remain in the gas phase and not solid phase, most of them can be removed at the beginning of the blowdown step, but the O_2 concentration of the effluent is much higher than that of ambient air. Therefore, in the PVSA II process, one more backfill step by the effluent from the first blowdown step of the CMS bed was added to the zeolite bed compared to the PVSA I process.

Mathematical Model

To understand the dynamic behaviors of a PVSA process, mathematical models were developed on the basis of the following assumptions: (1) the gas phase behaves as an ideal gas mixture, (2) radial concentration and temperature gradients are negligible, (3) thermal equilibrium between adsorbents and bulk flow is assumed, (4) the flow pattern is described by the axially dispersed plug-flow model, and (5) the pressure drop along the bed is measured using Ergun's equation. In numerous studies the significance of the radial gradient was neglected and similar assumptions in simulating the adsorption processes were also made.[19,20]

The component and overall mass balances for the bulk phase in the adsorption column are given by

$$-D_L\frac{\partial^2 c_i}{\partial z^2}+\frac{\partial(uc_i)}{\partial z}+\frac{\partial c_i}{\partial t}+\rho_p\left(\frac{1-\varepsilon}{\varepsilon}\right)\frac{\partial \overline{q_i}}{\partial t}=0 \qquad (1)$$

$$\frac{\partial(uC)}{\partial z}+\frac{\partial C}{\partial t}+\rho_p\left(\frac{1-\varepsilon}{\varepsilon}\right)\sum_{i=1}^{n}\frac{\partial \overline{q_i}}{\partial t}=0 \qquad (2)$$

Another characteristic of the adsorption process is the temperature variation caused by the heat of adsorption and desorption. To minimize the deviation in the prediction of high-purity product, the energy balance for the gas phase also includes the heat transfer to the column wall, expressed as

$$-K_L\frac{\partial^2 T}{\partial z^2}+\varepsilon\rho_g C_{pg}\frac{\partial(uT)}{\partial z}+(\varepsilon_t\rho_g C_{pg}+\rho_B C_{ps})\frac{\partial T}{\partial t}-\rho_B\sum_{i=1}^{n}(-\Delta\overline{H_i})\frac{\partial \overline{q_i}}{\partial t}+\frac{2h_i}{R_{Bi}}(T-T_w)=0 \qquad (3)$$

where ε_t is the total void fraction [$=\varepsilon+(1-\varepsilon)\times\alpha$], α is the particle porosity, and ρ_B is the bed density [$=(1-\varepsilon)\times\rho_p$].

To consider the heat loss through a wall and the heat accumulation in the wall, another energy balance for the wall of the adsorption bed was used

$$\rho_w C_{pw} A_w\frac{\partial T_w}{\partial t}=2\pi R_{Bi}h_i(T-T_w)-2\pi R_{Bo}h_o(T_w-T_{atm}) \qquad (4)$$

where $A_w=\pi(R_{Bo}^2-R_{Bi}^2)$.

In this study, the proposed PVSA process was operated by a combination of two cyclic sequences (Table 1). Therefore, an imbalance in the pseudo-cyclic operation among these beds was inevitable, although the effluents remained systematically connected to each other. In the simulation using gProms software, shown in Figure 1a, after retaining the temporal data from the effluent stream of the zeolite 10X bed during the adsorption step, these data were used in the pressurization and adsorption steps of the CMS bed. The temporal effluent data from the end of the CMS bed during its adsorption step was used in the first backfill step of the zeolite 10X bed. The temporal data from the CMS bed during the blowdown step were applied to the second backfill step of the zeolite 10X bed (Figure 1b). The two sets of boundary conditions were applied to the zeolite bed and CMS bed separately.

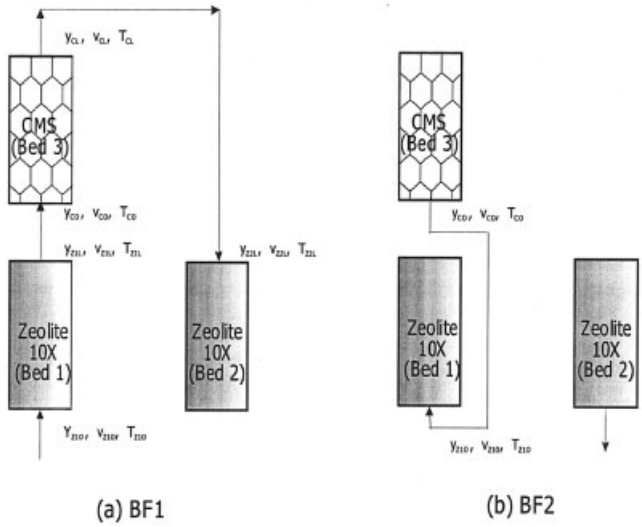

Figure 1. Simulation scheme of three-bed PVSA process with two zeolite beds and one CMS bed.
(a) BF1 and (b) BF2.

The boundary conditions for zeolite two-bed PVSA are as follows:

Boundary Conditions for Feed Pressurization (PR) and Adsorption (AD) Steps

$$-D_L\left(\frac{\partial c_i}{\partial z}\right)\Big|_{z=0}=u(c_i|_{z=0^-}-c_i|_{z=0^+}) \qquad \left(\frac{\partial c_i}{\partial z}\right)\Big|_{z=L}=0 \qquad (5a)$$

$$-K_L\left(\frac{\partial T}{\partial z}\right)\Big|_{z=0}=\varepsilon\rho_g C_{pg}u(T|_{z=0^-}-T|_{z=0^+}) \qquad \left(\frac{\partial T}{\partial z}\right)\Big|_{z=L}=0 \qquad (5b)$$

Boundary Conditions for First Backfill (BF1), Second Backfill (BF2), and Pressurizing Pressure Equalization (PPE) Step

$$-D_L\left(\frac{\partial c_i}{\partial z}\right)\Big|_{z=L}=u(c_i|_{z=L^+}-c_i|_{z=L^-}) \qquad \left(\frac{\partial c_i}{\partial z}\right)\Big|_{z=0}=0 \qquad (6a)$$

$$-K_L\left(\frac{\partial T}{\partial z}\right)\Big|_{z=L}=\varepsilon\rho_g C_{pg}u(T|_{z=L^+}-T|_{z=L^-}) \qquad \left(\frac{\partial T}{\partial z}\right)\Big|_{z=0}=0 \qquad (6b)$$

Table 2. Adsorption Isotherm and Diffusion Rate Parameters of N_2, O_2, and Ar on Zeolite 10X and CMS

Constants	Zeolite 10X			CMS		
	O_2	Ar	N_2	O_2	Ar	N_2
Equilibrium Parameters						
For LRC model						
k_1 (mol/g)	4.568×10^{-3}	3.697	2.330×10^{-3}	1.527×10^{-2}	2.042×10^{-2}	2.363×10^{-2}
k_2 (mol g^{-1} K^{-1})	-1.071×10^{-5}	-5.010×10^{-6}	-4.400×10^{-6}	-3.230×10^{-5}	-5.300×10^{-5}	-6.380×10^{-5}
k_3 (1/kPa)	9.866×10^{-5}	1.651×10^{-5}	1.674×10^{-8}	2.290×10^{-5}	23.97×10^{-5}	36.10×10^{-5}
k_4 (K)	578.9	869.7	3586	966.1	324.6	1444
k_5	3.552	3.184	1.384	1.187	1.646	1.692
k_6 (K)	−797.4	−665.6	−142.1	−106.0	−238.2	−270.0
Heat of adsorption, $-\Delta\bar{H}$ (kJ/mol)	9.623	10.46	16.32	13.81	14.23	13.39
Adsorption Rate Parameters						
For rate model						
D_{ci} (cm^2/s) in Eq. 14	0.0153	0.0147	0.0043			
C_i (1/s) in Eq. 15				0.024	0.000047	0.000090

Boundary Conditions for Depressurizing Pressure Equalization (DPE) and Countercurrent Vacuum Regeneration (VU) Steps

$$\left(\frac{\partial c_i}{\partial z}\right)\Big|_{z=0} = \left(\frac{\partial T}{\partial z}\right)\Big|_{z=0} = 0 \qquad \left(\frac{\partial c_i}{\partial z}\right)\Big|_{z=L} = \left(\frac{\partial T}{\partial z}\right)\Big|_{z=L} = 0 \tag{7}$$

The boundary conditions for a CMS one-bed PSA are as follows:

Boundary Conditions for PR and AD steps

$$-D_L\left(\frac{\partial c_i}{\partial z}\right)\Big|_{z=0} = u(c_i|_{z=0^-} - c_i|_{z=0^+}) \qquad \left(\frac{\partial c_i}{\partial z}\right)\Big|_{z=L} = 0 \tag{8a}$$

$$-K_L\left(\frac{\partial T}{\partial z}\right)\Big|_{z=0} = \varepsilon\rho_g C_{pg} u(T|_{z=0^-} - T|_{z=0^+}) \qquad \left(\frac{\partial T}{\partial z}\right)\Big|_{z=L} = 0 \tag{8b}$$

Boundary Conditions for Idle (ID), First Blowdown (BD1), and Second Blowdown (BD2) Steps

$$\left(\frac{\partial c_i}{\partial z}\right)\Big|_{z=0} = \left(\frac{\partial T}{\partial z}\right)\Big|_{z=0} = 0 \qquad \left(\frac{\partial c_i}{\partial z}\right)\Big|_{z=L} = \left(\frac{\partial T}{\partial z}\right)\Big|_{z=L} = 0 \tag{9}$$

Initial Condition for Fluid Flow

$$c_i(z, 0) = c_i^* \qquad \overline{q_i}(z, 0) = q_i^* \tag{10}$$

In this study, the adsorption beds were saturated with pure oxygen before each run.

Initial Condition for Heat Flow

$$T(z, 0) = T_{atm} \tag{11}$$

The pressure history during a PSA experiment at the feed or bed end was fitted by polynomials and used as a boundary condition for the overall mass balance.[21]

To consider the pressure drop effect across the bed, Ergun's equation was introduced as a momentum balance[22]

$$-\frac{dP}{dz} = a\mu u + b\rho u|u| \tag{12a}$$

$$a = \frac{150}{4R_p^2}\frac{(1-\varepsilon)^2}{\varepsilon^2} \qquad b = 1.75\frac{(1-\varepsilon)}{2R_p\varepsilon} \tag{12b}$$

where u is the interstitial velocity.

The multicomponent adsorption equilibrium was predicted by the following:

Loading Ratio Correlation (LRC) Model

$$q_i = \frac{q_{mi}B_iP_i^{n_i}}{1 + \sum_{j=1}^{n} B_jP_j^{n_j}} \tag{13}$$

where $q_{mi} = k_1 + k_2 \times T$, $B_i = k_3\exp(k_4/T)$, and $n_i = k_5 + k_6/T$.

In this study, the general LDF model assuming constant diffusivity was applied to the sorption rate of equilibrium separation bed (zeolite 10X)

$$\frac{\partial\overline{q_i}}{\partial t} = \omega_i(q_i^* - \overline{q_i}) \qquad \omega_i = \frac{15D_{ei}}{r_p^2} \tag{14}$$

In the case of the kinetic separation bed (CMS), the modified LDF model with concentration-dependent diffusivity was used.[23,24]

$$\frac{\partial\overline{q_i}}{\partial t} = \omega_i(q_i^* - \overline{q_i}) \qquad \omega_i = \frac{15D_{ei}}{r_p^2}$$

$$D_{ei} = C_i \cdot P_{ri}^{0.5}(1 + B_iP_i)^2 \tag{15}$$

Table 3. Characteristics of Adsorbent and Adsorption Bed

Characteristic	Zeolite 10X	CMS
Adsorbent		
Type	Pellet	Pellet
Average pellet size, R_p (cm)	0.115	0.28
Heat capacity, C_{ps} (J g^{-1} K^{-1})	1.13	0.96
Pellet density, ρ_p (g/cm^3)	1.1	0.90
Particle porosity, α	0.36	0.30
Bed density, ρ_B (g/cm^3)	0.82	0.63
Adsorption Bed		
Length, L (cm)	100	100
Inside radius, R_{Bi} (cm)	1.72	1.1
Outside radius, R_{Bo} (cm)	1.987	1.275
Heat capacity of column, C_{pw} (J g^{-1} K^{-1})	0.50	0.50
Density of column, ρ_w (g/cm^3)	7.83	7.83
Internal heat transfer coefficient, h_i (J cm^{-2} K^{-1} s^{-1})	3.85×10^{-3}	3.85×10^{-3}
External heat transfer coefficient, h_o (J cm^{-2} K^{-1} s^{-1})	1.42×10^{-3}	1.42×10^{-3}

Values of the adsorption isotherm and rate parameters of N_2, Ar, and O_2 on CMS and zeolite 10X, presented in Table 2, were very similar to the published data.[25-27]

Experimental

Zeolite 10X (Baylith WE-G 639; Bayer AG, Leverkusen, Germany) and CMS (3A; Takeda Chemicals, Tokyo, Japan) were used as adsorbents in the PVSA experiments. Characteristics of each adsorbent are listed in detail in Table 3. Before the experimental runs, the zeolite 10X was regenerated at 613 K overnight and the CMS at 423 K.

The zeolite 10X adsorption beds were made of stainless steel according to the following dimensions: length, 100 cm; ID, 3.44 cm; and wall thickness, 2.67 mm. The dimensions of the CMS bed were: length, 100 cm; ID, 2.2 cm; and wall thickness, 1.75 mm. Characteristics of the adsorption beds are listed in detail in Table 3.

The PVSA apparatus is shown in Figure 2. Three resistance temperature detectors (RTD, Pt 100 Ω) were installed 10, 50, and 80 cm from the feed end to measure temperature variations inside the bed. The flow rate was regulated by a mass flow controller and the total amount of feed flow was measured by a wet gas meter (Sinagawa Co., Tokyo, Japan). To keep the pressure of the adsorption bed constant during the adsorption step of the zeolite 10X bed, a back-pressure regulator was installed between the zeolite 10X bed and the CMS bed. An additional back-pressure regulator was also equipped at the end of the CMS bed to keep the pressure of the adsorption bed constant during the adsorption step of the CMS bed. Bed pressure was measured by pressure transducers equipped at the top and bottom of each bed.

The concentration of influent and effluent was analyzed by a mass spectrometer (QMG 422; Balzers Instruments, Lichtenstein). This analysis was confirmed by gas chromatography (HP 5890II; Hewlett–Packard, Palo Alto, CA). The system was fully automated by a personal computer running a control program, and all measurements including flow rate, pressure, temperature, and concentration were saved on the computer through the use of an AD converter.

A high-performance vacuum pump (DAH-60; Ulvac Kiko Inc., Kanagawa, Japan) was applied to bring the vacuum step of the zeolite 10X bed up to a level of 33.44–45.60 kPa, depending on the applied step time.

Each activated adsorbent bed was filled with pure O_2 (99.9+%) to prevent contamination from the outside air. Before running each experiment, the adsorption beds were vacuumed for 2 h. As an initial condition, the PVSA experiments were conducted at the bed saturated with pure O_2 (99.9+%) under the same level of adsorption pressure as used throughout the experiment. The temperatures of the feed, bed, and surroundings were kept in the range of 297 to 300 K during the experiments.

The ternary mixture (N_2/O_2/Ar; 78:21:1 vol %; DaeSung Industrial Gas Co., Seoul, Korea) was used as feed gas for the PVSA experiments. Specific operating conditions such as operating pressure, feed flow rate, and each cycle/step times can be found in Table 4.

Results and Discussion

Cyclic performance of PVSA I with a single blowdown/backfill step

Because the effluent from the zeolite 10X bed during the AD step at 253.31 kPa was supplied as feed gas for the PR and AD steps of the CMS bed, the CMS bed was pressurized to 162.12 kPa. The effluent from the AD step of the CMS bed was backfilled into the other zeolite 10X bed. Therefore, the pressure of the zeolite bed increased slightly after the VU step. It is noteworthy that the CMS bed underwent two cycles for every one cycle of the zeolite bed because each of the zeolite beds and the CMS bed was tied to the same cycle time. To prevent confusion of the number of cycles, the cycle number of the

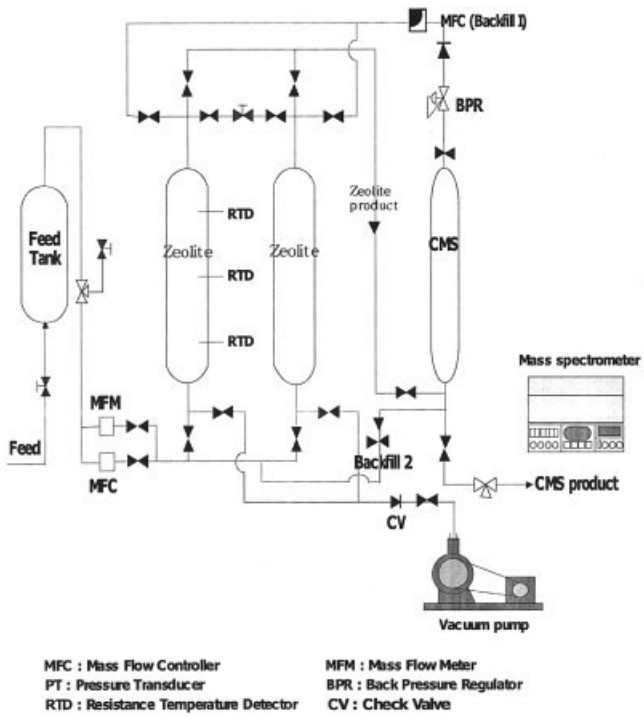

Figure 2. Apparatus for a three-bed PVSA process.

Table 4. Operating Conditions for PVSA for Air Separation and O_2 Purification

Run No.	Process	Adsorption Pressure of Zeolite 10X Bed (kPa)	Adsorption Pressure of CMS Bed (kPa)	Vacuum Pressure of Zeolite 10X Bed (kPa)	Feed Rate (LSTP/min)	PVSA I* (BD-PR-AD-ID-BD-PR-AD-ID) PVSA II* (BD2-PR-AD-ID-BD1-BD2-PR-AD-ID-BD1)
1	PVSA I	253.31	162.12	38.50	2.0	40-20-20-20-40-20-20-20 (Base step time)
2			174.28	33.44		40-**30**-**10**-20-40-**30**-**10**-20
3			131.72	45.60		40-**10**-**30**-20-40-**10**-**30**-20
4	PVSA II		167.19	39.52		30-20-20-20-10-30-20-20-20-10 (Base step time)
5			177.32	33.44		30-**30**-**10**-20-10-30-**30**-**10**-20-10
6			136.79	44.58		30-**10**-**30**-20-10-30-**10**-**30**-20-10

*The step sequence and time for the CMS bed were presented.

PVSA process was determined by the cycle of the zeolite 10X bed.

The temperature excursion in the zeolite 10X bed was around 5 K, whereas in the CMS bed it was 1 K. Because the experiment was performed under O_2 saturated conditions, the temperature history of the CMS bed showed an increase during the initial cycles. The temperature cyclic steady state for the process was reached at 15 cycles.

Figure 3 shows the cyclic variation of the mean concentration produced by the zeolite 10X and CMS beds at Run 1 (Table 4). The concentration variation curves also reached a cyclic steady state after nearly 15 cycles. In previous studies, the two-bed O_2 PSA purifier packed with CMS reached the cyclic steady state after only three cycles[17] when the binary feed (O_2/Ar; 95:5 vol %) was used. However, in this study, the cyclic steady state of the CMS bed was delayed because of the cyclic steady state of the zeolite 10X bed.

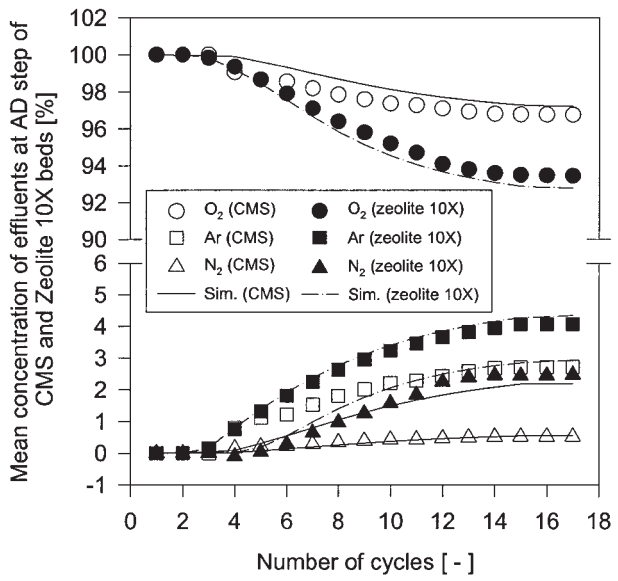

Figure 3. Cyclic variation of O_2 purity and Ar/N_2 impurities produced from the BD step of CMS bed during the cyclic operation of PVSA I at base operating condition (Run 1).

As noted in Figure 3, the zeolite 10X bed, as a bulk air separator, produced 93.5% O_2 with 2.5% N_2 and 4% Ar impurities. The product purity was higher than that of conventional O_2 VSA at similar operating conditions because the zeolite bed was partially pressurized by the BF step with the concentrated O_2 from the AD step of the CMS bed. Because such product quality was supplied to the CMS bed, the purity of O_2 purified through the CMS bed was about 96.8% at the cyclic steady state (Figure 3). The amount of N_2 impurity significantly decreased to the level of 4000–5000 ppm (=0.4–0.5 vol %) and Ar impurity also decreased from 4 to 2.7%. The results simulated by the dynamic model corresponded with the results of the experiment in both the equilibrium and kinetic separation beds.

The simulated concentration profiles of each adsorbate at the gas phase of the zeolite 10X bed are presented in Figures 4a to 4c. At the end of the AD step (Figure 4a), the mass-transfer zone (MTZ) of each adsorbate became steeper as that of each gas propagated to the bed end. In addition, the concentration of Ar at the bed end became slightly higher than that of N_2. At the end of the BF step after the DPE and VU steps (Figure 4b), the MTZ of N_2 was observed retreating to the feed end with a broader shape than it had at the VU step and O_2 and Ar accumulated in higher concentrations at the bed end. Finally, at the end of the PPE step (Figure 4c), each MTZ retreated further to the feed end bearing the concave shape of N_2 MTZ and the convex shape of O_2 and Ar MTZs.

Figures 4d and 4e show the axial concentration profiles along the CMS bed at the end of each step. As noted in Figure 4d, the O_2 concentration profile at the end of the PR step was formed at the concave shape around the bed end because the Ar and N_2 in the gas phase were concentrated at that location of the bed. Moreover, because a higher concentration of Ar than N_2 was supplied to the CMS bed and the diffusion rate of Ar was much slower than that of N_2, the concentration of Ar at this step was higher than that of N_2. At the end of the AD step (Figure 4e), the gas-phase concentration of each adsorbate was nearly constant at each of the axial positions because the adsorbed phase was nearly saturated with highly concentrated O_2. This result means that a tangible amount of the impurities in the gas phase was removed during the AD step time. In addition, because the

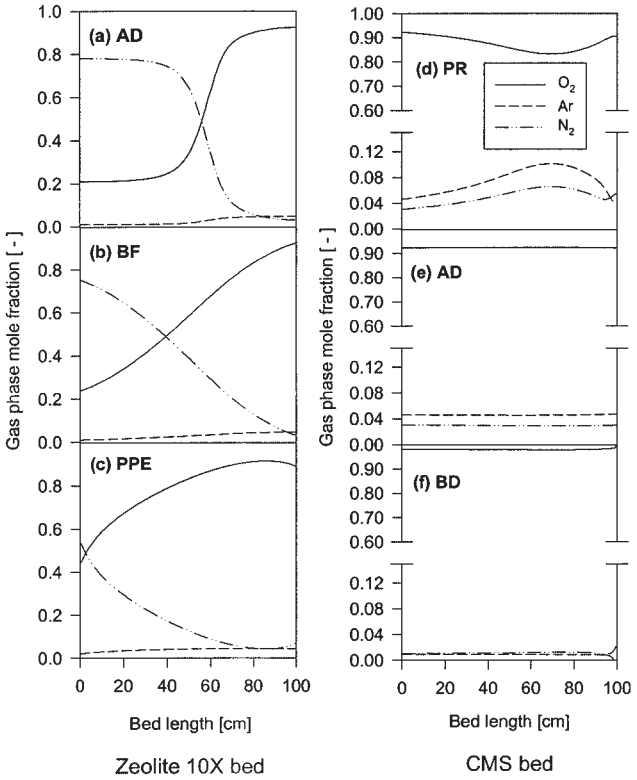

Figure 4. Simulated O_2 concentration profiles in the gas phase at (a) AD, (b) BF, and (c) DPE steps of zeolite 10X bed and (d) PR, (e) AD, and (f) BD steps of CMS bed during the PVSA I operation at base operating condition (Run 1).

concentration of O_2 during the AD step in the CMS bed was relatively high, the effluent BF gas could improve the performance of the zeolite bed (Figure 4c). At the end of the ID step, the MTZs of N_2 and Ar at the bed end increased slightly because the small amount of O_2 diffused into the solid phase. Then, high-purity O_2 was produced at the end of the BD step (Figure 4f). As shown in Figure 3, a greater amount of Ar than N_2 was included in the product because the Ar with the slower diffusion rate remained in the gas phase.[23,28] In addition, the MTZs of Ar and N_2 crossed over at the vicinity of the bed end in the BD step because the desorption of N_2 from the adsorbed phase was quicker than that of Ar.

Effect of adsorption step time in the CMS bed on adsorption dynamics in PVSA I

As shown in Figure 4, the AD step in the CMS bed played a key role in removing the N_2 and Ar impurities from the zeolite bed. In addition, because this step was connected to the zeolite bed as a BF step, the AD step time in the CMS bed contributed to the purity and recovery of the product in the process.

Therefore, the effect of the AD step time of the CMS bed on O_2 purity and recovery was studied at the fixed AD step time of the zeolite bed, 40 s, which corresponded to the sum of the PR and AD step times of the CMS bed (Table 1). Although the AD step time of one zeolite bed was fixed to 40 s, the AD step of the CMS bed was tied to the VU and BF steps of the other zeolite bed. Therefore, a decrease in the AD step time of the CMS bed caused an increase in the VU step time (higher vacuum pressure in Table 4) as well as an decrease in the BF step time of the zeolite bed.

As shown in Figure 5a, as the AD step time of the CMS bed decreased from 30 to 10 s (the PR step time of the CMS bed increased from 10 to 30 s), the purity of both the zeolite 10X and the CMS beds decreased linearly because of the reduced amount of backfill gas in the zeolite bed and the diminished time for impurity removal in the CMS bed. The effect of the AD step time of the CMS bed on the purity of each bed was slightly greater in the zeolite bed than in the CMS bed. As shown in Figure 5b, with a decrease in the AD step time, O_2 recovery substantially increased to 85% because the extended PR step time of the CMS bed led to increased adsorption pressure in the CMS bed. Compared to the change of recovery in the AD step time, the effect of the AD step time of the CMS bed on purity was relatively small because the extended VU step time in the zeolite bed could compensate somewhat for the reduced BF gas (Table 4).

Figure 6 shows the axial concentration profiles at the AD step in the CMS bed and at the BF step in the zeolite 10X bed. In Figure 6a, the MTZs of the components did not completely proceed to the CMS bed end within the AD step time of 10 s. Therefore, this AD step time was not sufficient to remove the

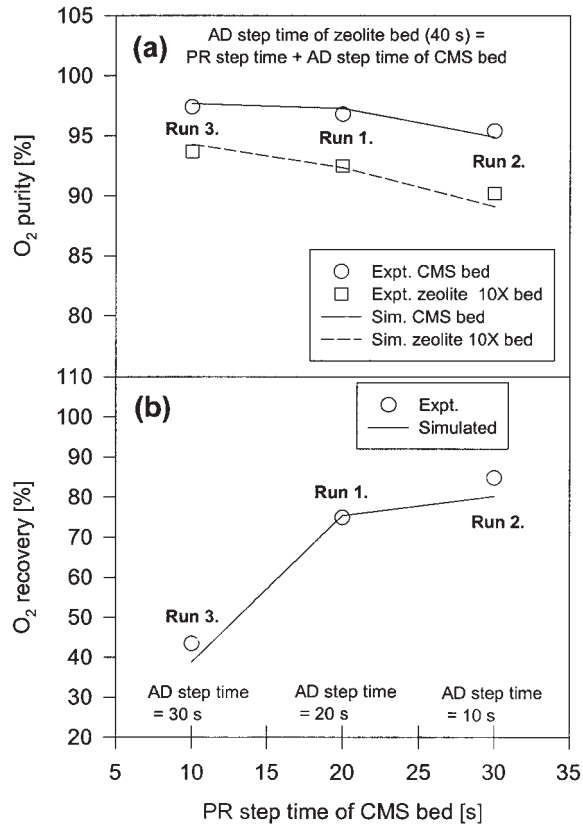

Figure 5. Effect of PR and AD step times of CMS bed on (a) O_2 purity and (b) O_2 recovery at base adsorption pressure and base feed flow rate condition (Runs 1 to 3).

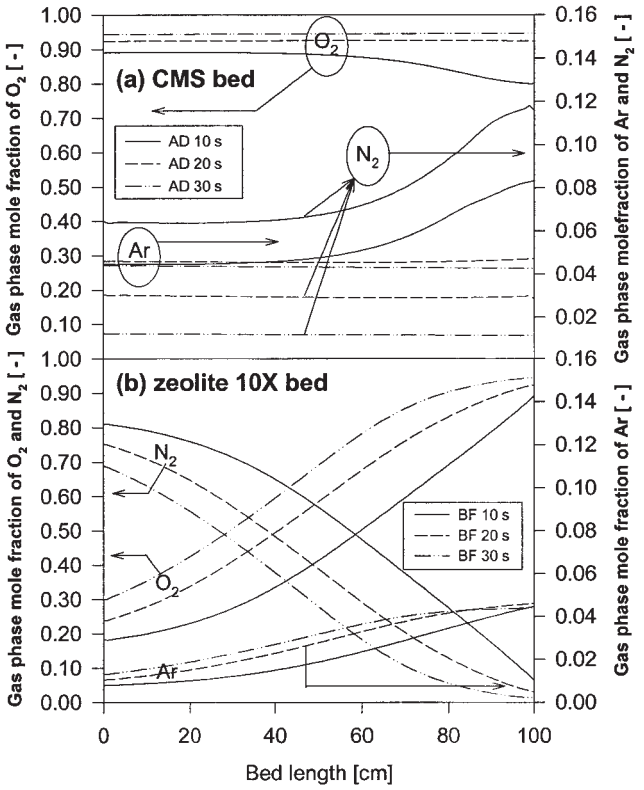

Figure 6. Axial concentration profiles along the bed in the gas phase at the end of (a) BF step of zeolite 10X bed and (b) AD step of CMS bed at base adsorption pressure and base feed flow rate condition (Runs 1 to 3).

impurities of N_2 and Ar in the CMS bed. Furthermore, N_2 acted as the primary impurity in the product because the concentration of N_2 in the bed was higher than that of Ar under that step time. However, over 20 s, all the MTZs were linear along the CMS bed, showing a lower concentration of N_2 than Ar. The amount of N_2 significantly decreased with an increase in AD step time.

The corresponding step in the zeolite bed is shown in Figure 6b. At the BF step time of 10 s (corresponding to the AD step time of 10 s in the CMS bed), the MTZs of O_2 and Ar were unfavorable because a relatively large amount of N_2 was supplied from the CMS bed. However, as the BF step time increased, the MTZ of N_2 retreated to the feed end and the MTZs of O_2 and Ar became favorable because the highly concentrated O_2 feed backfilled from the AD step of the CMS bed was supplied from the bed end. Consequently, an increased AD step time in the CMS bed led to an increase in the purity of the O_2 product through the AD step of the zeolite bed, although the recovery decreased (Figure 5) because a greater amount of the gas supplied from the zeolite bed was used in the BF step.

Cyclic performance of PVSA II with double blowdown/backfill steps

As to be expected, most of the impurities of the product from the CMS bed in PVSA I were recorded at the initial period of production time (Figure 4). To improve the product purity of O_2 in PVSA II, a fractionation step of the product from the CMS bed was added to PVSA I, as shown in Table 1.

Unlike PVSA I, an additional BF step (BF2) was added in the zeolite 10X bed and two consecutive BD steps (BD1 and BD2) were applied to the CMS bed. The effluents from the AD and BD1 steps in the CMS bed were used to partially pressurize the zeolite 10X bed at the BF1 and BF2, respectively. In comparison to PVSA I, PVSA II was operated at the same total cycle time, adsorption pressure, and feed flow rate (Table 4), all based on the zeolite bed.

Figure 7 shows the representative cyclic behaviors of the CMS and zeolite 10X beds at Run 4, comparing the experiment's effluent O_2 purity and Ar/N_2 impurities with the calculated results. Similar to the PVSA I process, the concentration variation reached a cyclic steady state after nearly 17 cycles. However, in Run 4 of PVSA II, O_2 purity from the CMS bed increased noticeably to 98.8%. Compared with PVSA I's performance in Figure 3, it is noteworthy that the amount of N_2 in the zeolite bed and the amount of Ar in the CMS bed were reduced significantly in PVSA II. In the final product of PVSA II, the mole fraction of Ar impurity contained in the product decreased to 1.2%, whereas that of N_2 was several tens of ppm. In addition, O_2 purity from the zeolite 10X bed exceeded 96% with 3.6% Ar and 0.4% N_2, recognized as the theoretical limitation of the adsorption equilibrium process.

Figures 8a–8c show the axial concentration profile at the end of each step along the zeolite 10X bed in PVSA II. As shown in Figures 8a–8c, the MTZs of all the components in PVSA II were similar to those in PVSA I (Figures 4a–4c). However, the axial concentration amount of N_2 at the bed end was less than that of Ar in the entire PVSA II process, which stands in marked contrast to PVSA I (Figures 4a–4c).

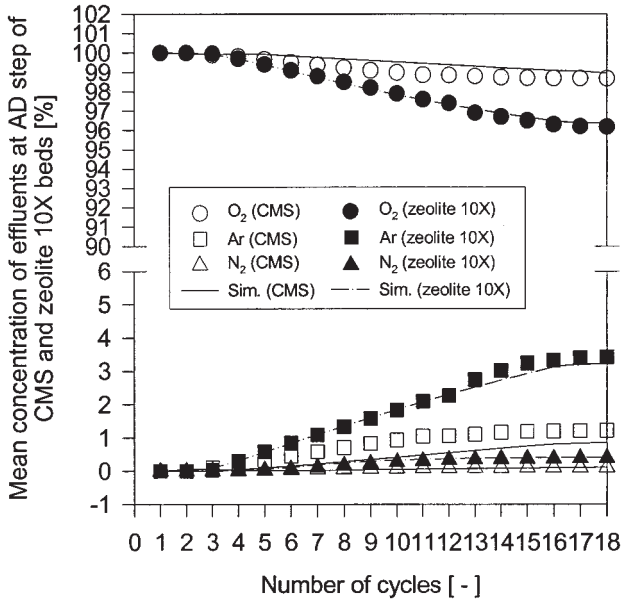

Figure 7. Cyclic variation of O_2 purity and Ar/N_2 impurities produced from BD2 step of CMS bed during cyclic PVSA operation for 99% O_2 generation at base operating condition (Run 4).

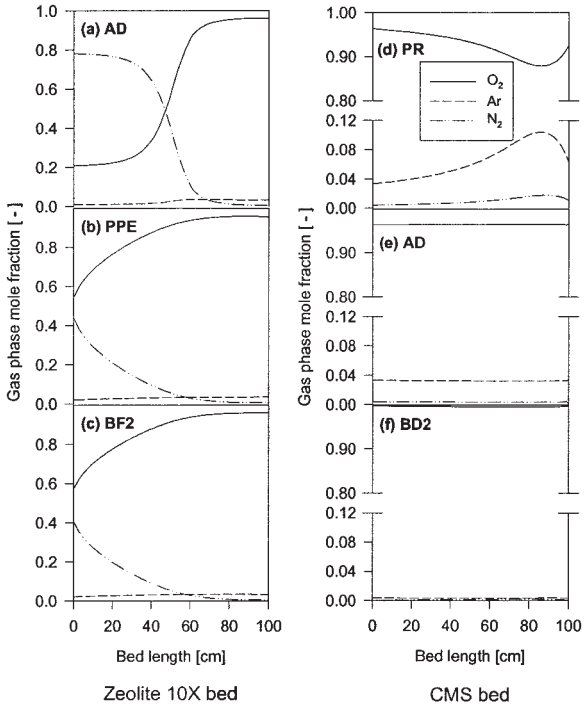

Figure 8. Simulated O_2 concentration profiles in the gas phase at (a) AD, (b) PPE, and (c) BF2 steps of zeolite 10X bed and (d) PR, (e) AD, and (f) BD2 steps of CMS bed during the PVSA II operation at base operating condition (Run 4).

At the end of the PR and AD steps in Figure 8a, the MTZs of N_2 in PVSA II propagated to the bed end more slowly than those in PVSA I. This was mainly caused by the second backfill gas, which was composed of highly concentrated O_2. In Figure 8b, like Figure 4c, the concave shape of axial N_2 concentration at the bed end was formed at the end of the PPE step even though the bed had for the most part been regenerated through previous regeneration steps such as VU and BF1. This concave shape had a detrimental effect on the production of high-purity O_2 because the N_2 impurity near the bed end was contained in the product at the AD step of the next cycle. However, the concave shape of N_2 MTZ and the convex shape of O_2 MTZ at the bed end disappeared at the end of the BF2 step (Figure 8c) because the high-purity O_2 from the CMS bed was reintroduced at the bed end of the zeolite 10X bed.

Figures 8d–8f show the axial concentration profile at the end of each step along the CMS bed in PVSA II. Compared to the axial concentration profiles of PVSA I in Figure 4d, the roll-ups of N_2 and Ar at the PR step occurred at the bed end as shown in Figure 8d. In addition, because the amount of N_2 impurity supplied from the zeolite 10X bed was noticeably smaller (Figure 8a), the concentration profiles of N_2 throughout the steps were much lower than those in Figure 4. Therefore, as shown in Figure 8e, the CMS bed in PVSA II was saturated with a higher concentration of O_2 at the end of the AD step than was that in PVSA I. Moreover, by introducing the two-stage blowdown step, considerable amounts of Ar and N_2 were removed from the CMS bed through the BD1 step, which was operated under pressures ranging from adsorption pressure to medium pressure. Simultaneously, the effluent gas at this step was supplied to the zeolite bed through the BF2 step (Figure 8c). As a result, high-purity O_2 of >99% could be produced through the BD2 step of the CMS bed (Figure 8f) and the bed was kept clean for the next step.

Effect of adsorption step time in the CMS bed on adsorption dynamics in PVSA II

The effect of AD step time in the CMS bed on O_2 purity and recovery in PVSA II was studied to compare to the results with those of PVSA I in Figure 5.

As shown in Figure 9a, when the AD step time of the CMS bed increased from 10 to 30 s, the purity of both the zeolite 10X and CMS beds increased linearly, similar to the results noted in Figure 5a. Consequently, oxygen with 99.2% purity was produced at the AD step time of 30 s because a greater amount of impurities had been removed from the CMS bed and a greater amount of O_2 had been supplied to the zeolite bed through the BF1 step. Therefore, the O_2 purity of the zeolite 10X bed also increased to 97% under this AD step time. However, as shown in Figure 9b, the recovery diminished as the PR step time decreased because the decreased PR step time of the CMS bed led to a lower adsorption pressure in the bed.

Compared with the results of PVSA I, the deviation of the

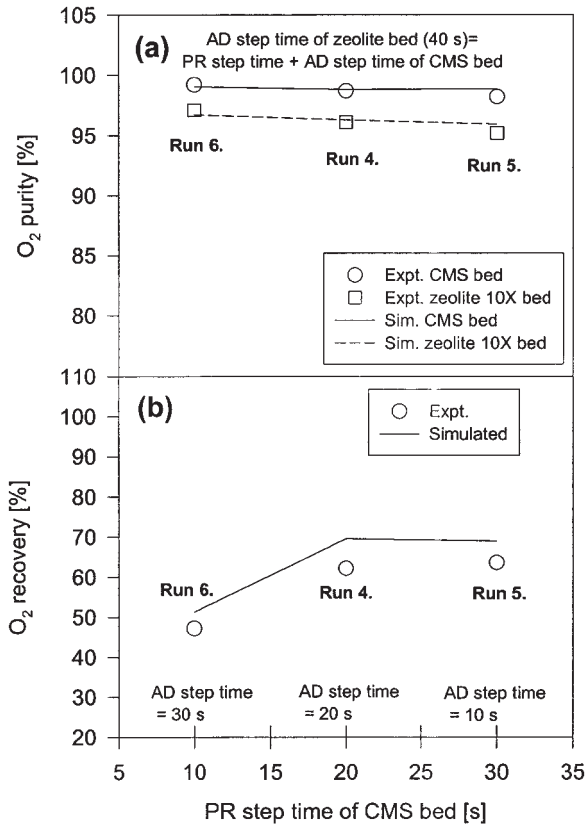

Figure 9. Effect of PR and AD step times of CMS bed on (a) O_2 purity and (b) O_2 recovery at base adsorption pressure and base feed flow rate condition (Runs 4 to 6).

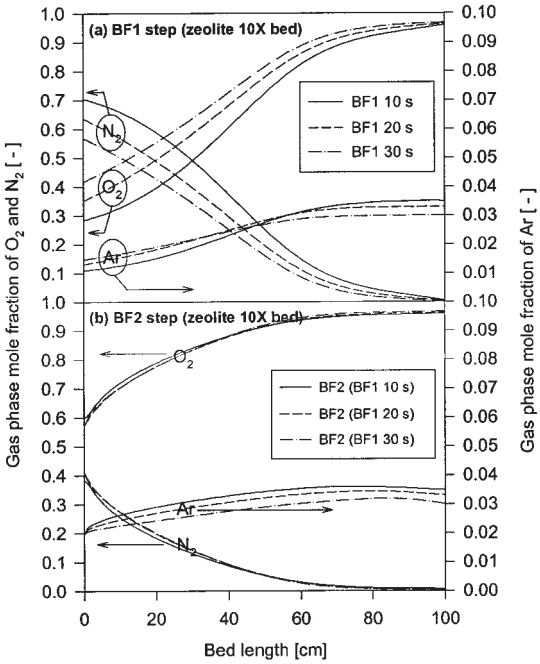

Figure 10. Axial gas phase concentration profiles along the bed at the end of (a) BF1 and (b) BF2 steps of zeolite 10X bed at base adsorption pressure and base feed flow rate condition (Runs 4 to 6).

BF2 step time was fixed to 10 s.

simulated recovery in the PVSA II is slightly higher than that in the PVSA I. Because one more backfill step and one more blowdown step were applied to the PVSA II, respectively, more errors in these steps, especially velocity, might be accumulated in the simulation. It is clear that PVSA II can produce a higher purity of O_2 than PVSA I under the same conditions in cyclic time, pressure, and feed flow rate. However, the recoveries of Runs 4 and 5 were about 10–20% lower than the corresponding Runs 1 and 2 in PVSA I as a result of the BD1 step in the CMS bed and the BF2 in the zeolite bed. In the case of Run 6, it is noted that O_2 with 99.2% purity could be produced at a higher recovery than the corresponding Run 3 in PVSA I.

Figure 10 shows the axial concentration profiles of the BF1 and BF2 steps in the zeolite bed. Similar to the results in Figure 6b, as the BF step time increased, the MTZs of each component retreated to the feed end (Figure 10a). However, unlike the results in Figure 6b, the MTZs of O_2 and Ar maintained their favorable shape even at a BF1 step time of 10 s and the MTZs of Ar crossed near the center of the bed. This was because the BF2 step following from the CMS bed led to a more highly saturated O_2 condition throughout the bed.

When the same BF2 step time was applied to the above three BF1 conditions, the MTZ of each adsorbate further retreated to the feed end (Figure 10b). The BF1 step of 30 s showed the lowest MTZ of Ar and the highest MTZ of O_2 at the BF2 step. Moreover, because the convex shape of the O_2 MTZ and the concave shape of the N_2 MTZ at the end of the PPE step (Figures 4c and 8b) disappeared at the end of the BF2 step, the zeolite bed had conditions favorable to the effective supplying of better feed to the CMS bed.

Figure 11 shows the axial concentration profiles of the BD1 and BD2 steps in the CMS bed of PVSA II. At the end of the BD1 step (Figure 11a), the O_2 mole fraction in the gas phase was in the range of 97–98% and the N_2 mole fraction was <0.005%. The lower mole fraction of impurities at the end of the BD1 step was achieved with an increase in AD step time because the AD step in the CMS bed worked to remove the impurities. After the BD2 step, as shown in Figure 11b, the O_2 mole fraction exceeded 99.5% and almost the same concentrations of impurities remained regardless of AD step time conditions in the CMS bed. Therefore, the CMS bed was ready to purify feed under more favorable conditions in the PVSA II process.

Work is currently under way to optimize the process by using a parametric study and to assess economical analysis by using the pilot-plant study.

Conclusions

The three-bed PVSA process was refined to surpass 94% O_2 purity from ambient air using adsorption technology. By using two zeolite 10X beds and one CMS bed, the PVSA process

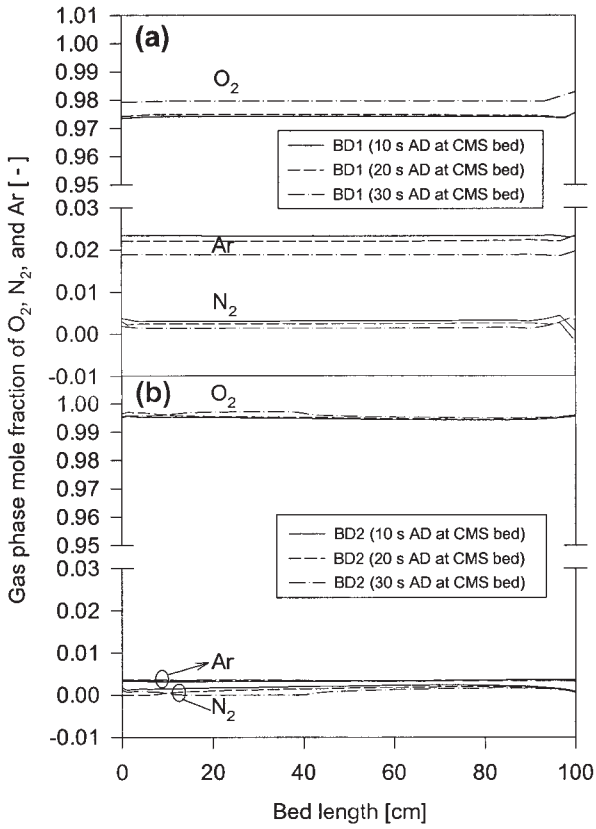

Figure 11. Axial gas phase concentration profiles along the bed at the end of (a) BD1 and (b) BD2 steps of CMS bed at base adsorption pressure and base feed flow rate condition (Runs 4 to 6).

BD1 and BD2 step times were fixed to 10 and 30 s, respectively.

could produce O_2 with a purity $> 94\%$ directly from the ambient air. In addition, the nonisothermal dynamic model successfully predicted the cyclic behaviors in the experiment.

In the PVSA I process, which adopted a single stage of the blowdown/backfill step, the cyclic steady state was reached after about 14–15 cycles. In the case of the bulk air separator, the zeolite 10X bed, O_2 with a purity of 90.2–93.7% was produced, whereas the impurities of N_2 and Ar were 2.5–6.3 and 3.5–4.2%, respectively. This O_2 product was further purified to 95.4–97.4% with a recovery of 43.4–84.8% in the CMS bed. The amount of N_2 in the product was 4000–5000 ppm during the PVSA I process.

The effect of the PR and AD step times in the CMS bed on the performance of the process was analyzed at the fixed AD step time of the zeolite 10X bed. As a consequence, the increased AD step time of the CMS bed contributed to an increase in O_2 purity because the AD step of the CMS bed acted as an impurity-removal step and a greater amount of backfill gas was supplied to the zeolite 10X bed. However, the excessive AD step time of the CMS bed led to a significant decrease in recovery because the backfill and vacuum step times of the zeolite bed increased simultaneously.

In the PVSA II process, two-stage blowdown/backfill steps were adopted to increase O_2 purity by fractionating the O_2 product from the BD step of the CMS bed. The zeolite 10X bed produced O_2 with a purity of 95.2–97.1%. This process overcame the purity limit of common adsorption processes using zeolites because of the two-stage backfill steps supplied from the CMS bed. Thus, PVSA II could produce an O_2 purity of 98.2–99.2% with a recovery of 47.2–63.6% through the CMS bed. Also, the amount of N_2 impurity decreased to <100 ppm. Similar to PVSA I, the increased AD step time of the CMS bed led to an increase in O_2 purity and a decrease in O_2 recovery in the PVSA II process. However, because more highly concentrated O_2 was supplied from the zeolite bed in PVSA II rather than in PVSA I, the CMS bed in PVSA II could be kept fairly clean after the production step, regardless of the applied AD step time in the CMS bed. Therefore, the CMS bed had more favorable conditions for the purification of feed in PVSA II.

In the near future, further results will be presented of the parametric study to directly produce a maximum of 99.8+% O_2 from air by using the proposed PVSA processes.

Acknowledgments

The financial support of the Carbon Dioxide Reduction & Sequestration R&D Center (C002-0103-001-1-0-0) is gratefully acknowledged.

Notation

A_W = cross-sectional area of the wall, cm^2
B = equilibrium parameter for Langmuir—Freundlich model, kPa^{-1}
c_i = i component concentration in bulk phase, mol/cm^3
C_{pg}, C_{ps}, C_{pw} = gas, pellet, and wall heat capacity, respectively, J $g^{-1}\cdot K^{-1}$
D_e = effective diffusivity defined by solid diffusion model, cm^2/s
D_L = axial dispersion coefficient, cm^2/s
h_i = internal heat-transfer coefficient, J cm^{-2} K^{-1} s^{-1}
h_o = external heat-transfer coefficient, J $cm^{-}\cdot$ K^{-1} s^{-1}
$-\Delta H$ = average heat of adsorption, J/mol
k = parameter for Langmuir and LRC models
K_L = axial thermal conductivity, J cm^{-1} s^{-1} K^{-1}
L = bed length, cm
n = dimensionless equilibrium parameter for Langmuir–Freundlich model
P = total pressure, kPa
P_r = reduced pressure
q, q^*, $\bar{q}$ = amount adsorbed, equilibrium amount adsorbed, and average amount adsorbed, respectively, mol/g
q_m = equilibrium parameter for Langmuir–Freundlich model, mol/g
R = gas constant, J mol^{-1} K^{-1}
R_p = radius of pellet, cm
R_{Bi}, R_{Bo} = inside and outside radius of the bed, respectively, cm
t = time, s
T_{atm} = temperature of atmosphere, K
T, T_w = pellet or bed temperature and wall temperature, respectively, K
u = interstitial velocity, cm/s
y_i = mole fraction of species i in gas phase
z = axial distance in bed from the inlet, cm

Greek letters

α = particle porosity
ε, ε_t = voidage of adsorbent bed and total void fraction, respectively
ρ_g, ρ_p, ρ_B, ρ_w = gas density, pellet density, bulk density, and bed wall density, respectively, g/cm^3
ω = LDF coefficient, s^{-1}
μ = viscosity, Pa·s

Subscripts

B = bed
i = component i
p = pellet
g = gas phase
s = solid phase
w = wall

Literature Cited

1. Kumar R. Vacuum swing adsorption process for oxygen production—A historical perspective. *Sep Sci Technol.* 1996;31:877-893.
2. Rege SU, Yang RT. Limits for air separation by adsorption with LiX zeolite. *Ind Eng Chem Res.* 1997;36:5358-5365.
3. Rei β G. Status and development of oxygen generation processes on molecular sieve zeolites. *Gas Sep Purif.* 1994;8:95-99.
4. Kawai M, Kaneko T. Present state of PSA air separation in Japan. *Gas Sep Purif.* 1989;3:2-6.
5. Wilson SJ, Webley PA. Cyclic steady-state axial temperature profiles in multilayer, bulk gas PSA—The case of oxygen VSA. *Ind Eng Chem Res.* 2003;41:2753-2765.
6. Jiang L, Biegler LT, Fox VG. Simulation and optimization of pressure-swing adsorption systems for air separation. *AIChE J.* 2003;49:1140-1157.
7. Mendes AMM, Costa CAV, Rodrigues AE. Oxygen separation from air by PSA: Modeling and experimental results—Part I: Isothermal operation. *Sep Purif Technol.* 2001;24:173-188.
8. Yang RT. *Gas Separation by Adsorption Processes*. Boston, MA: Butterworth; 1987.
9. Ruthven DM, Farooq S, Knaebel KS. *Pressure Swing Adsorption*. New York, NY: VCH; 1994.
10. Zayaraman A, Yang RT, Cho SH, Bhat SG, Choudary VN. Adsorption of nitrogen, oxygen and argon on Na-CeX zeolites. *Adsorption.* 2002; 8:271-278.
11. Ko D, Siriwardane R, Bigler RT. Optimization of a pressure-swing adsorption process using zeolite 13X for CO_2 sequestration. *Ind Eng Chem Res.* 2003;42:339-348.
12. Miller GW, Theis CF. Secondary oxygen purifier for molecule sieve oxygen concentrator. U.S. Patent No. 4 813 979; 1989.
13. Miller GW, Theis CF. Molecular sieve oxygen concentrator with secondary oxygen purifier. U.S. Patent No. 4 880 443; 1989.

14. Knaebel KS, Kandynin A. Pressure swing adsorption system to purify oxygen. U.S. Patent No. 5 226 933; 1993.
15. Rege SU, Yang RT. Kinetic separation of oxygen and argon using molecular sieve carbon. *Adsorption.* 2000;6:15-22.
16. Hayashi S, Kawai M, Kaneko T. Dynamics of high purity oxygen PSA. *Gas Sep Purif.* 1996;10:19-23.
17. Jee JG, Kim MB, Lee CH. Pressure swing adsorption processes to purify oxygen using a carbon molecular sieve. *Chem Eng Sci.* 2005; 60:869-882.
18. Lee CH. Apparatus for producing oxygen and method for controlling the same. PCT/KR2004/001209; 2004.
19. Jee JG, Lee JS, Lee CH. Air separation by a small-scale two-bed medical O_2 PSA. *Ind Eng Chem Res.* 2001;40:3647-3658.
20. Kikkinides ES, Yang RT. Effects of bed pressure drop on isothermal and adiabatic adsorber dynamics. *Chem Eng Sci.* 1993;48:1545-1555.
21. Jee JG, Park H, Haam S, Lee CH. Effects of nonisobaric and isobaric steps on O_2 pressure swing adsorption for an aerator. *Ind Eng Chem Res.* 2002;41:4383-4392.
22. Yang J, Park MW, Chang JW, Ko SM, Lee CH. Effects of pressure drop in a PSA process. *Korean J Chem Eng.* 1998;15:211-216.
23. Bae YS, Lee CH. Sorption kinetics of eight gases on a carbon molecular sieve at elevated pressure. *Carbon.* 2005;43:95-107.
24. Bae YS, Moon JH, Ahn H, Lee CH. Effect of adsorbate properties on adsorption mechanism in a carbon molecular sieve. *Korean J Chem Eng.* 2004;21:712-720.
25. Ruthven DM, Raghavan NS, Hassan MM. Adsorption and diffusion of nitrogen and oxygen in a carbon molecular sieve. *Chem Eng Sci.* 1986;41:1325-1332.
26. Chen YD, Yang RT, Uawithya P. Diffusion of oxygen, nitrogen, and their mixtures in carbon molecular sieve. *AIChE J.* 1994;40: 577-585.
27. Sorial GA, Granville WH, Daly WO. Adsorption equilibria for oxygen and nitrogen gas mixtures on 5 Å molecular sieves. *Chem Eng Sci.* 1983;38:1517-1523.
28. Qinglin H, Farooq S, Karimi IA. Binary and ternary adsorption kinetics of gases in carbon molecular sieves. *Langmuir.* 2003;19: 5722-5734.

Manuscript received Nov. 23, 2004, and revision received Mar. 10, 2005.